Separation Science and Technology
Publication details, including instructions for authors and subscription information:
http://www.informaworld.com/smpp/title~content=t713708471

Experimental and Numerical Investigation of Two-Dimensional CO_2 Adsorption/Desorption in Packed Sorption Beds Under Non-ideal Flows

H. Mohamadinejad[a]; J. C. Knox[b]; J. E. Smith[a]
[a] Department of Chemical Engineering, University of Alabama, Huntsville, Alabama, USA [b] Marshall Space Flight Center, National Aeronautics and Space Administration, Huntsville, Alabama, USA

Online publication date: 10 September 2003

To cite this Article Mohamadinejad, H. , Knox, J. C. and Smith, J. E.(2003) 'Experimental and Numerical Investigation of Two-Dimensional CO_2 Adsorption/Desorption in Packed Sorption Beds Under Non-ideal Flows', Separation Science and Technology, 38: 16, 3875 — 3904
To link to this Article: DOI: 10.1081/SS-120024710
URL: http://dx.doi.org/10.1081/SS-120024710

SEPARATION SCIENCE AND TECHNOLOGY
Vol. 38, No. 16, pp. 3875–3904, 2003

Experimental and Numerical Investigation of Two-Dimensional CO_2 Adsorption/Desorption in Packed Sorption Beds Under Non-ideal Flows

H. Mohamadinejad,[1] J. C. Knox,[2] and J. E. Smith[1,*]

[1]Department of Chemical Engineering, University of Alabama, Huntsville, Alabama, USA
[2]Marshall Space Flight Center, National Aeronautics and Space Administration, Huntsville, Alabama, USA

ABSTRACT

The experimental results of CO_2 adsorption and desorption in a packed column indicated that the concentration wave front at the center of the packed column differs from those close to the wall of column filled with adsorbent material even though the ratio of column diameter to the particle size is greater than 20.[1] The comparison of the experimental results with one-dimensional model of packed column shows that to simulate the average breakthrough in a packed column, a two-dimensional (radial and axial) model of packed column is needed.[2] In this article, the mathematical model of a nonslip flow through a packed column 2 inches in diameter and 18 inches in length filled with 5A

*Correspondence: J. E. Smith, Department of Chemical Engineering, University of Alabama, Huntsville, AL, USA; E-mail: smithje1@email.vah.edu.

DOI: 10.1081/SS-120024710
0149-6395 (Print); 1520-5754 (Online)

www.dekker.com

MARCEL DEKKER, INC.
270 Madison Avenue, New York, New York 10016

zeolite pellets is presented. The comparison of experimental results of CO_2 adsorption and desorption for the mixed and central breakthrough of the packed column with numerical results is also presented.

INTRODUCTION

The one-dimensional mathematical model approach to simulate a packed column indicates the lack of accuracy of concentration prediction away from the center of column.[1] The experimental results on the concentration measurement show a substantial difference between the mixed and the central concentration in adsorption and desorption of CO_2 and H_2O on 5A Zeolite pellets. Numerous experimental data suggests that the channeling effect is significant even for a large ratio of column diameter to the particle size (d/d_p).[3–7] Benenati and Brosilow[3] indicated that channeling is very pronounced at the ratio of column diameter to the particle size of less than 20. Cohen[6] showed that for the ratio of column diameter to the particle size of less than about 30 the a peak velocity of at about one particle diameter away from the wall; the velocity here ranged from 30 to 100% greater than the bulk velocity. The contribution to the radial temperature difference is mostly comes by different rate of adsorption along the cross section of the packed column which is based on the channeling effect in a nearly adiabatic packed column. In the adsorption of H_2O on 5A zeolite in a nearly adiabatic packed column the channeling effect is more pronounce for H_2O than CO_2 even after few hours when the cross-sectional temperature is constant.[2] This observation is coherent with the fact that the heat transfer front is ahead of mass transfer front in a packed column. Therefore, a non-Darcian flow model (two-dimensional flow) has been developed to simulate the adsorption and desorption processes in a packed column. Finite-differencing numerical technique was used to solve the system of partial differential equations. For a packed bed the porosity varies with distance from the wall. Near the wall the porosity is higher than the bulk of the bed. This increases the permeability. A few particles away from the wall, the porosity equals the free stream value.[3,8] As a consequence of the porosity increase in the vicinity of the wall, the velocity of the flow parallel to the wall increases as the wall is approached and goes through a maximum before it decreases to zero (to satisfy the no-slip condition). In general, this leads to a net increase in flux, i.e., to the phenomenon called channeling.[9] In this study, channeling effect on momentum, energy, and material balances was considered to be important enough so that two-dimensional adsorption in the packed bed must be modeled.

Marcel Dekker, Inc.
270 Madison Avenue, New York, New York 10016

Mathematical Model for Nonisothermal Multicomponent Adsorption in a Packed Bed

Momentum, heat, and mass balance equations can model the two-dimensional dynamic bed behavior. The mathematical model was used to estimate the breakthrough curve for a certain constituent in the bulk gas. In return, this enabled us to obtain the necessary parameters for predicting the transient behavior of the temperature profile and concentration of the gas for different initial parameters such as inlet concentration, temperature, and the fluid velocity.

These equations were solved numerically by finite difference methods, namely the Newman methods.[10] A FORTRAN code was written to find the numerical solutions to the transient equations.

Two-Dimensional Adsorption Mathematical Model

The complicated molecular diffusion of a component in a mixture is described by the Stefan–Maxwell equation. For the single component diffusion in a mixture, however, the diffusion coefficient D_{mi} for the component is approximately related to the binary coefficients by the following relationship.[11]

$$D_{mi} = \frac{1 - y_i}{\sum_{j \neq i}^{n} \frac{y_j}{D_{i,j}}} \tag{1}$$

For binary mixtures at low pressure, $D_{i,j}$ can be estimated as it suggested by Slattery and Bird.[12]

Diffusion Model for Zeolite

The rate of adsorption into the adsorbent pellets assumed to be approximated by the linear driving force approximation model,

$$\frac{\partial \bar{q}_i}{\partial t} = k_{ef} a_s (q_i^* - \bar{q}_i) \tag{2}$$

Where k_{ef} may be obtained by experimental procedure and a_s is the interfacial surface area. The justification of assuming a linear diving force to model the adsorbed concentration in the solid phase has been well established by other researchers.[13–16]

MARCEL DEKKER, INC.
270 Madison Avenue, New York, New York 10016

Component concentration can be modeled as:

$$\frac{\partial C_i}{\partial t} = D_{effi,x}\frac{\partial^2 C_i}{\partial x^2} - \frac{\partial (uC_i)}{\partial x} + D_{effi,r}\frac{\partial}{r\partial r}\left(\frac{r\partial C_i}{\partial r}\right) - \frac{(1-\varepsilon)}{\varepsilon}\frac{\partial \bar{q}_i}{\partial t} \tag{3}$$

Boundary and initial condition as:

$$\begin{aligned} &for\ t < 0\ C_i = C_{i,0}\ for\ 0 \le x \le L\ and\ 0 \le r \le R_i \\ &for\ t \ge 0\ C_i = C_{i,x0}\ at\ x = 0\ and\ 0 \le r \le R_i \\ &for\ t \ge 0\ \frac{\partial C_i}{\partial x} = 0\ at\ x = L\ and\ 0 \le r \le R_i \\ &for\ t \ge 0\ \frac{\partial C_i}{\partial r} = 0\ at\ r = 0\ and\ r = R \end{aligned}$$

The energy balance for the gas phase can be modeled as:

$$\rho_g C_{pg}\frac{\partial T_g}{\partial t} = k_{f,x}\frac{\partial^2 T_g}{\partial x^2} - \frac{\partial u T_g}{\partial x} + \frac{k_{f,r}}{r}\frac{\partial}{\partial r}\left(\frac{r\partial T_g}{\partial r}\right) - \frac{1-\varepsilon}{\varepsilon}h_s a_s (T_g - T_s) \tag{4}$$

Boundary and initial condition as:

$$\begin{aligned} &at\ t < 0, T_g = T_{g,0}\ for\ 0 \le x \le L\ and\ 0 \le r \le R_i \\ &at\ t \ge 0, T_g = T_{0,x}\ for\ x = 0\ and\ 0 \le r \le R_i \\ &at\ t \ge 0, \frac{\partial T_g}{\partial x} = 0\ for\ x = L\ and\ 0 \le r \le R_i \\ &at\ t \ge 0, \frac{\partial T_g}{\partial r} = 0\ at\ r = 0\ for\ 0 \le x \le L \\ &at\ t \ge 0, k_{f,r}\frac{\partial T_g}{\partial r} = h_w(T_w - T_g)\ at\ r = R\ for\ 0 \le x \le L \end{aligned}$$

The energy balance for the solid phase can be modeled as:

$$\rho_s C_{ps}\frac{\partial T_s}{\partial t} = k_{s,x}\frac{\partial^2 T_s}{\partial x^2} + \frac{k_{s,r}}{r}\frac{\partial}{\partial r}\left(\frac{r\partial T_s}{\partial r}\right) + h_s a_s (T_g - T_s) + \sum_{i=1}^{n}\Delta H_i\frac{\partial \bar{q}_i}{\partial t} \tag{5}$$

Marcel Dekker, Inc.
270 Madison Avenue, New York, New York 10016

Boundary and initial condition as:

$$at\ t < 0, T_s = T_{s,0}\ for\ 0 \le x \le L\ and\ 0 \le r \le R_i$$

$$at\ t \ge 0, T_s = T_{0,x}\ for\ x = 0\ and\ 0 \le r \le R_i$$

$$at\ t \ge 0, \frac{\partial T_s}{\partial x} = 0\ for\ x = L\ and\ 0 \le r \le R_i$$

$$at\ t \ge 0, \frac{\partial T_s}{\partial r} = 0\ at\ r = 0\ and\ r = R\ for\ 0 \le x \le L$$

Rate of adsorption $\partial\bar{q}/\partial$t can be substituted in the above equation.

The energy balance for the wall can be written as:

$$\rho_w C_{pw} \frac{\partial T_w}{\partial t} = 2\pi R_i h_w (T_g - T_w) - 2\pi R_o h_o (T_w - T_o)$$
$$InitialCondition \tag{6}$$
$$at\ t < 0, T_w = T_{w,0}$$

Bed Energy Equation Based On Effective Conductivity

$$(\varepsilon\rho_g C_{pg} + (1-\varepsilon)\rho_s C_{ps})\frac{\partial T}{\partial t} = \varepsilon k_{eff,x}\frac{\partial^2 T}{\partial x^2} + \varepsilon\frac{k_{eff,r}}{r}\frac{\partial}{\partial r}\left(\frac{r\partial T}{\partial r}\right)$$
$$- \varepsilon u\rho_g C_{pg}\frac{\partial T}{\partial x} + (1-\varepsilon)\sum_{i=1}^{n}\Delta H_i\frac{\partial\bar{q}_i}{\partial t} \tag{7}$$

Boundary and initial condition as:

$$at\ t < 0, T = T_0\ for\ 0 \le x \le L\ and\ 0 \le r \le R_i$$

$$at\ t \ge 0, T = T_{0,x}\ for\ x = 0\ and\ 0 \le r \le R_i$$

$$at\ t \ge 0, \frac{\partial T}{\partial x} = 0\ for\ x = L\ and\ 0 \le r \le R_i$$

$$at\ t \ge 0, \frac{\partial T}{\partial r} = 0\ at\ r = 0\ for\ 0 \le x \le L$$

$$at\ t \ge 0, k_{eff,r}\frac{\partial T}{\partial r} = h_w(T_w - T|_{r=R})\ for\ r = R_i$$

The governing momentum equation for cylindrical beds for fully developed flow[17] is:

$$\frac{\partial P}{\partial x} = -\rho_g C u^2 - \frac{\mu}{K}u + \frac{1}{r}\frac{\mu}{\varepsilon}\frac{\partial}{\partial r}\left(r\frac{\partial u}{\partial r}\right),$$
$$Boundary\ Conditions \tag{8}$$
$$u = -\frac{K_\infty}{\mu}\frac{\partial P}{\partial x}\ at\ r = 0\ and\ u = 0\ at\ r = R_i$$

where ε is the porosity, and K and C are the permeability and inertial coefficient, which are related to the porosity and the type of porous materials. In the above equation, the second term is the inertial effect, which accounts for additional pressure drop resulting from interpore mixing found at higher Reynolds numbers.[17,18] The third term is the Darcian force representing the pressure loss due to the presence of solid particles. The last term is the viscous shear force representing the resistance to the flow caused by sheer stress along the solid boundary. This term accounts for the no-slip boundary condition at the solid boundary. In this study, the entrance effect was not considered since the flow is fully developed after one-to two-particle distance from the entrance.[17]

Porosity Variation

$$\varepsilon = \varepsilon_\infty \lfloor 1 + a \exp(-by/d_p \rfloor \tag{9}$$

where ε_∞ is the free-stream porosity, y is the distance from the wall, d is the particle diameter, and a is taken to be 1.4.[9] b is experimental parameters that depend on packing and particle size, it varies from 2 to 8.

The empirical coefficients K and C, which are given by the relations developed by Ergun[18] for flow in a packed bed, are:

$$K = \frac{d^2\varepsilon^3}{150(1-\varepsilon)^2} \tag{10}$$

$$C = \frac{1.75(1-\varepsilon)}{d\varepsilon^3} \tag{11}$$

The variable C and K, are both a function of the bed porosity and particle diameter, d. The porosity in a packed bed increases from the center of bed, free-stream porosity, to a maximum of 1 at the bed-wall boundary. This increase is confined within few particle diameters from the wall.[3,8]

In the above two-dimensional equations, the term that represents the radial diffusion, is

$$\frac{1}{r}\frac{\partial}{\partial r}\left(\frac{r\partial C}{\partial r}\right) \tag{12}$$

where C is a variable. By carrying out the derivative, it can be recast into

$$\frac{1}{r}\frac{\partial C}{\partial r} + \frac{\partial^2 C}{\partial r^2} \tag{13}$$

Marcel Dekker, Inc.
270 Madison Avenue, New York, New York 10016

At the center where $r = 0$, the first term is not finite. But

$$Limit_{r\to 0}\left(\frac{1}{r}\frac{\partial C}{\partial r}\right) = \frac{\partial^2 C}{\partial r^2} \tag{14}$$

by L'Hospital's rule. Therefore, the term, Eq. 12, in a two-dimensional form for the center point is replaced by

$$\frac{1}{r}\frac{\partial}{\partial r}\left(\frac{r\partial C}{\partial r}\right) = 2\frac{\partial^2 C}{\partial r^2} \tag{15}$$

Therefore, the diffusional term in the discretized forms of two-dimensional PDEs at center grid is replaced by Eq. 15.

Calculation of Thermal Conductivity for Two-Dimensional Flow

In this study, two different equations were used to calculate the effective conductivity in the packed bed. One is based on the works of Kunii and Smith,[19] and the other one is based on the experimental work of Fahien.[20]

The effective thermal conductivity in the axial and radial direction, $k_{eff,x}$ and $k_{eff,r}$, are related as,

$$\begin{aligned} k_{eff,x} &= k_\circ + k_{f,x} \\ k_{eff,r} &= k_\circ + k_{f,r} \end{aligned} \tag{16}$$

In the above equations, the radial and axial conductivity is the combination of two terms. The first term is the stagnation conductivity, which varies from a bulk conductivity to fluid conductivity with distance from the center to the column wall. Therefore, it depends on the porosity variation, which also is a function of bed parameters. The second term is due to the dynamic or dispersion conductivity, which incorporates the mixing, caused by flow through the particles. This conductivity can be calculated by theoretical equations. Based on the work of Kunii and Smith the following equations result.

Stagnant Conductivity k_o

Kunii and Smith[19] presented theoretical equations for estimating the stagnant conductivity, k_o. The stagnant conductivity can be found If k_s, solid thermal conductivity, is given.

$$\frac{k_\circ}{k_f} = \varepsilon + (1-\varepsilon)/[\phi + (2/3)(k_f/k_s)] \tag{17}$$

where k_f is the thermal conductivity of fluid and ϕ is the contribution of solid-to-solid heat transfer through fluid film around a contacting point of neighboring particles. ϕ is given by

$$\begin{aligned} &\phi = \phi_2 + (\phi_1 - \phi_2)[(\varepsilon - .26)/.216] \\ &for\ .476 \geq \varepsilon \geq .26 \\ &\phi = \phi_1 \\ &for\ \varepsilon > .476 \\ &\phi = \phi_2 \\ &for\ \varepsilon < .26 \end{aligned} \tag{18}$$

where ϕ_1 and ϕ_2 are given in a schematic form and are being interpolated linearly in tabularform in the computer program.

Effective Radial Conductivity $k_{f,r}$

The thermal conductivity in radial direction for packed bed is given by Baron[21] as

$$C_{pg}\rho_f u/k_{f,r} = N_{Pe_H} = 8 - 10 \tag{19}$$

where N_{PeH} is Peclet number. Therefore, the effective thermal conductivity in radial direction would be.[22]

$$\frac{k_{eff,r}}{k_f} = \frac{k_\circ}{k_f} + (\alpha\beta)N_{\mathrm{Re}_P}N_{\mathrm{Pr}} \tag{20}$$

where $(\alpha\beta) = 1/\mathrm{N}_{\mathrm{Pe}_\mathrm{H}} = 0.1$ to 0.125

Effective Axial Conductivity $k_{eff,x}$

A similar equation can be derived for effective thermal conductivity in the axial direction.[23]

$$\frac{k_{eff,x}}{k_f} = \frac{k_\circ}{k_f} + \lambda N_{\mathrm{Re}_P}N_{\mathrm{Pr}} \tag{21}$$

where $\lambda = 0.5$ to 1.0

Incorporating the effects of porosity variation into the effective conductivity, the effective conductivity reduces to[24]

$$\frac{k_{eff,r}}{k_f} = (1 + a' \exp(-bR))\frac{k_\circ}{k_f} + (\alpha\beta)\frac{l(R)}{d}N_{\mathrm{Re}_P}N_{\mathrm{Pr}} \tag{22}$$

where $(\alpha\beta) = 1/\mathrm{N}_{\mathrm{Pe}_\mathrm{H}} = 0.1$ to 0.15

Marcel Dekker, Inc.
270 Madison Avenue, New York, New York 10016

And in the axial direction,

$$\frac{k_{eff,x}}{k_f} = (1 + a' \exp(-bR)) \frac{k_\circ}{k_f} + \lambda \frac{l(R)}{d} N_{\mathrm{Re}_P} N_{\mathrm{Pr}} \tag{23}$$

where $\lambda = 0.5$ to 1.0 and a' is chosen such that k_o/k_f equals 4 at the wall as velocity becomes zero. The variation of dispersion, mixing length, is

$$\frac{l(R)}{d} = R_t - r \quad for\ R_t - r \leq 1 \tag{24}$$

where R_t is tube diameter. An expression similar to porosity variation was used to predict the mixing length variation.[24]

Calculation of Mass Diffusivity for Two-Dimensional Flow

A similar theoretical approach can be taken for the calculation of diffusivity in the radial and axial direction.

Effective Diffusivity

Effective diffusivity follows the same expression as in thermal conductivity.

$$\begin{aligned} D_{eff,x} &= D_\circ + D_{f,x} \\ D_{eff,r} &= D_\circ + D_{f,r} \end{aligned} \tag{25}$$

Effective Radial Diffusivity $D_{f,r}$

The effective diffusivity in the radial direction by analogy to heat transfer is

$$\frac{D_{eff,r}}{D_f} = \frac{D_\circ}{D_f} + (\alpha\beta) N_{\mathrm{Re}_P} N_{SC,} \tag{26}$$

where $(\alpha\beta) = 1/N_{\mathrm{Pe}_H} = 0.1$ to 0.125.

Effective Axial Diffusivity $D_{eff,x}$

A similar equation can be derived for effective diffusivity in the axial direction,

$$\frac{D_{eff,x}}{D_f} = \frac{D_\circ}{D_f} + \lambda N_{\mathrm{Re}_P} N_{SC} \tag{27}$$

where $\lambda = 0.5$ to 1.0.

MARCEL DEKKER, INC.
270 Madison Avenue, New York, New York 10016

Incorporating the effects of porosity variation into the effective diffusivity, the effective diffusivity reduces to[24]

$$\frac{D_{eff,r}}{D_f} = (1 + a' \exp(-bR)) \frac{D_\circ}{D_f} + (\alpha\beta) \frac{l(R)}{d} N_{\mathrm{Re_p}} N_{Sc,} \tag{28}$$

where $(\alpha\beta) = 1/N_{Pe_n} = 0.1$ to 0.15.

And in the axial direction,

$$\frac{D_{eff,x}}{D_f} = (1 + a' \exp(-bR)) \frac{D_\circ}{D_f} + \lambda \frac{l(R)}{d} N_{\mathrm{Re_p}} N_{Sc,} \tag{29}$$

where $\lambda = 0.5$ to 1.0.

Effective Radial Thermal Conductivity Based on Fahin Equations

In contrast to the weak effect of mass diffusion on radial mass fraction, the thermal conductivity profile has a strong effect on both temperature and mass adsorption. A thermal conductivity profile for different ratio of d_t/d_t was approximated by Fahien[20] as:

$$k_{eff,r} = < k > \left(k^*_\circ + 3(k^*_M - k^*_\circ) \frac{r^2}{r_M^2} + 2(k^*_M - k^*_\circ) \frac{r^3}{r_M^3} \right)$$

$$\times 0 \le \mathrm{r} \le r_M$$

$$k_{eff,r} = < k > \left(k^*_M - (k^*_M - k^*_W) \frac{r - r_M}{1 - r_M} \right) r > r_M$$

$$k^*_M = \frac{3.0 - .9k^*_\circ r_M^2 - k^*_W \dfrac{r_M^3 - 3r_M^2 + 2}{1 - r_M}}{1 + r_M + .1r_M^2} \tag{30}$$

$$r_M = 1 - \frac{2}{\alpha}$$

$$\alpha = d_t/d_p$$

where K_o* is the effective radial conductivity at the center of the column wall, K_M* is the maximum effective thermal conductivity, K_W* the effective thermal conductivity near the wall, $<K>$ is the average effective thermal conductivity, and r_M is the location of maximum in conductivity profile. These conductivities are obtained using the Argo and Smith equation[25]

using the void fraction values as a function of radial position. According to Argo and Smith

$$k_{eff} = \varepsilon\left[k_g + \frac{d_p C_{pg} G}{N_{Pe}\varepsilon} + 4\left(\frac{\sigma}{2-\sigma}\right)d_p(0.173)(T_a^3/100^4)\right] + (1-\varepsilon)\frac{hk_s d_p}{2k_s + hd_p} \tag{31}$$

where σ is the emissivity of solid particle, T_a is the average temperature. In the above equation

$$h = h_c + h_r + h_p$$

$$h_c = 1.95 C_{pg} G N_{\mathrm{Pr}}^{-2/3} N_{\mathrm{Re}}^{-.51} \quad \mathrm{N_{Re}} < 350$$

$$h_c = 1.06 C_{pg} G N_{\mathrm{Pr}}^{-2/3} N_{\mathrm{Re}}^{-.41} \quad \mathrm{N_{Re}} < 350$$

$$h_r = \frac{k_r(2k_s + hd_p)}{d_p k_s}$$

$$k_r = 4\left(\frac{\sigma}{2-\sigma}\right)d_p(.173)\left(\frac{T_a^3}{100^4}\right)$$

$$h_p = \frac{k_p(2k_s + hd_p)}{d_p k_s}$$

$$\log_{10} k_p = 1.76 + .0129 k_s/\sigma$$

Effective Radial Diffusivity Based on Fahin Equations

$$D_{eff,r} = < D > \left(D_\circ^* + 3\left(D_M^* - D_\circ^*\right)\frac{r^2}{r_M^2} + 2\left(D_M^* - D_\circ^*\right)\frac{r^3}{r_M^3}\right) \times 0 \le \mathrm{r} \le r_M$$

$$D_{eff,r} = < D > \left(D_M^*\frac{r - r_M}{1 - r_M}\right) r > r_M$$

$$D_M^* = \frac{3.0 - .9 D_\circ^* r_M^2}{1 + r_M + .1 r_M^2} \tag{32}$$

D_M* is obtained from work of Fahin and Smith[26] to be

$$D_\circ^* = 9/8 V_\circ(1 + 4.85\alpha^{-2})$$

where V_o is velocity at the center of packed bed.

MARCEL DEKKER, INC.
270 Madison Avenue, New York, New York 10016

The effective thermal conductivity in the wall layer of thickness $R_P = d_P/2$, k_{ew}, is defined and h_w is considered as a correction factor based on the difference $k_{eff,r}$ and k_{ew}.[27]

$$\frac{k_{ew}}{k_f} = \frac{k_{ew0}}{k_f} + \frac{1}{\dfrac{1}{\alpha_w N_{\mathrm{Pr}} N_{Re}} + \dfrac{1}{h_w^* d_p / k_f}} \tag{33}$$

where α_w denotes the contribution of fluid mixing in the wall layer and is taken as 0.2, and h_W represents the heat transfer coefficient of the thermal boundary layer, which develops on the wall surface. This becomes dominant at high $N_{Re,p}$ and is given by a Blasius type equation as:[28]

$$h_w^* d_p / k_f = C(N_{\mathrm{Pr}}^{1/3} N_{\mathrm{Re}}, p^{3/4}) \tag{34}$$

where C is an experimental coefficient with value of 0.1 to 0.2.[27] k_{ew0} is obtained by the following equation, similarly to Eq. 17.

$$\frac{k_{ew0}}{k_f} = \varepsilon_w + (1 - \varepsilon_w)/[\phi_w + (2/3)(k_f/k_s)] \tag{35}$$

where ε_w denotes void fraction in the wall layer of about 0.7.

Table 1. Model inputs for two-dimensional flow.

Flow rate	28.04 standard, L/min
Inlet pressure	15.587 psia
CO_2 partial pressure	6.14 mm Hg
H_2O partial pressure	6.0352 mm Hg
Initial temperature	77°F
Bed void fraction	0.35
Interfacial surface area	635
Pellet density	0.75 lb/ft^3
CO_2 mass-transfer coefficient	0.02 ft/hr
CO_2 heat of adsorption	18,000.0 Btu/lb-mole
N_2 Heat of adsorption	8988 Btu/lb-mole
Specific heat (pellet)	0.2 Btu/lb-°F
Thermal conductivity (pellet)	0.1 Btu/ft^2-hr-°F

NUMERICAL SOLUTION

The solution to the nonequilibrium, nonisothermal adsorption/desorption problem must be found numerically. In this study, for a two-component mixture, the numerical model would involve the solution of several coupled differential equations: one mass balance equation, two mass balance of rate equations (solid phase), one total mass balance equation, one momentum equation, one heat balance of fluid flow equation, one heat balance of solid equation, and one equation for heat balance for a wall.

The finite difference technique, which is mostly used for processes with varying boundary and initial conditions, is a more convenient method to use for solving the coupled, partial differential equations (PDE). In this work, the PDEs were discretized by first-or second-order differences in time and spatial dimensions. The set of discretized finite difference equations was solved simultaneously by the implicit method. Based on the

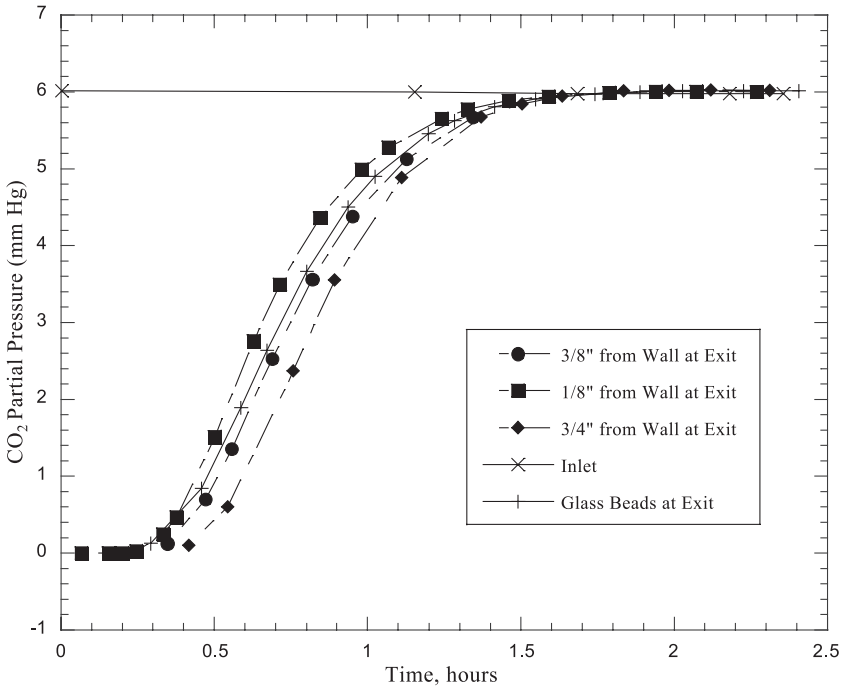

webcolor

Figure 1. CO_2 breakthrough for various radial positions.

MARCEL DEKKER, INC.
270 Madison Avenue, New York, New York 10016

stiffness and the sharpness of momentum equations and the mass and heat transfer fronts, the implicit method of Newman was used to simulate the adsorption process.[10,29]

The examination of convergence or the rate of convergence of the numerical methods used in this study ***relied*** on actual testing of the iterative methods. Since the set of equations is both coupled and nonlinear, an analytical procedure for determination of convergence can not be used.

In Newman's method, the number of grids could be reduced to 50 grids and the time-step ranges adjusted from 12 to 60 seconds. The iteration was stopped if $(C_{n+1} - C_n)/C_{n+1}$ was less than 1.0E-4 for each grid point.

The stability and the rate of convergence in these PDEs are mostly affected by rate of adsorption, which are related to isotherms. At low concentrations, the adsorption affinity of N_2 on 5A zeolite is less than CO_2 by about an order of magnitude. The adsorption affinity of CO_2 is also less than H_2O by about an order of magnitude.[2] The steep concentration gradient of H_2O relative to CO_2 and CO_2 relative to N_2 causes the rate of

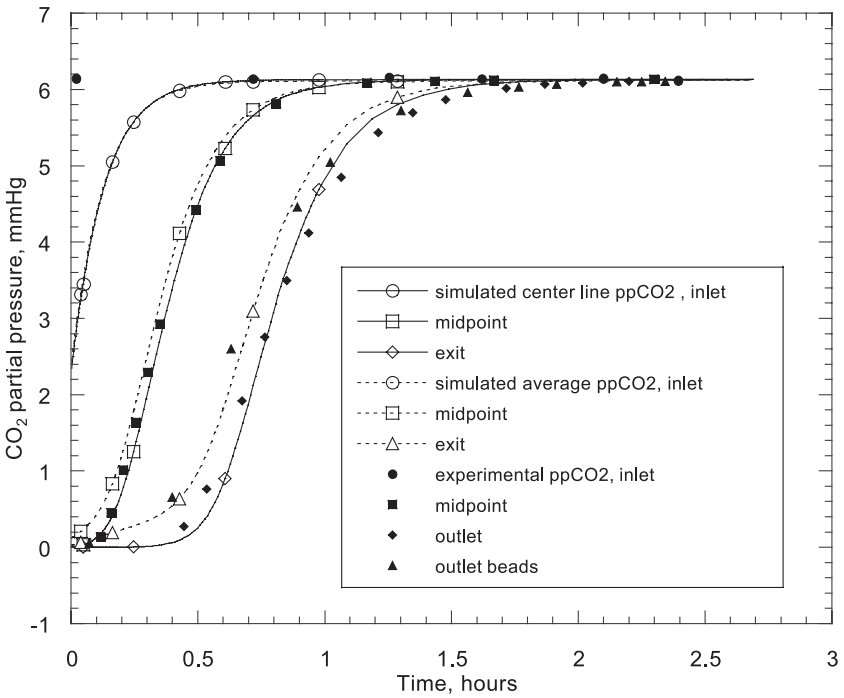

Figure 2. CO_2 breakthrough comparison test with two-dimensional model results.

Marcel Dekker, Inc.
270 Madison Avenue, New York, New York 10016

convergence to be smaller for H_2O in comparison to CO_2 and smaller for CO_2 in comparison to N_2. For single component adsorption of H_2O and CO_2 on 5A zeolite, the time step for an H_2O run must be much less than the time step used for a CO_2 run, otherwise the numerical model would not converge. Also, the number of iterations for convergence with a given time step is much larger for H_2O than CO_2. The second most important criterion is the inclusion of a diffusion rate into the mass and energy balance equations. The implementation of diffusion coefficients makes the PDEs parabolic functions and, in turn, causes the equations to be more stable. This is because diffusion exercises a smoothing effect on the PDEs.[30]

Test Apparatus

Verification of the numerical models is accomplished with test data from the molecular sieve material bench test (MSMBT), a Marshall Space

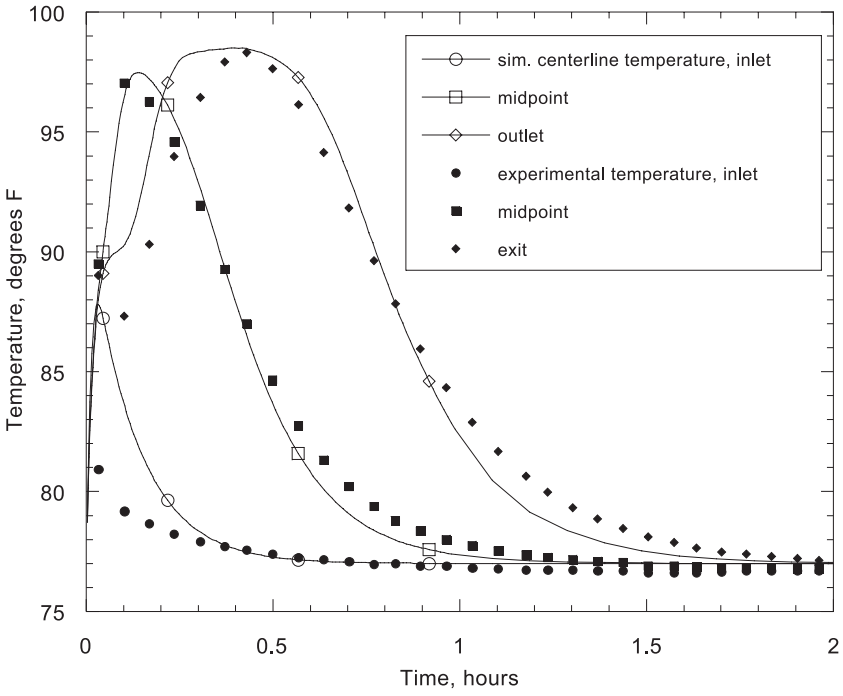

Figure 3. CO_2 single component temperature comparisons with two-dimensional model results.

MARCEL DEKKER, INC.
270 Madison Avenue, New York, New York 10016

Flight Center apparatus. The test apparatus consists of a small packed column 2 inches in diameter and 10 or 20 inches long, depending on the configuration. Instrumentation of the column includes temperature probes and sampling tubes for measurement at sorbent material endpoints and intermediate points. Continuous measurements of the exit CO_2 partial pressures, and all temperatures are recorded. A gas chromatograph is used to capture the breakthrough at interior bed locations. The MSMBT is fully described elsewhere.[2] Any significant changes made in the test configuration are discussed in the following sections, as appropriate.

The MSMBT is used to obtain data empirically that is not available otherwise or not reliable in the open literature, such as heat of adsorption and lumped mass-transfer coefficients. Testing to obtain empirical data is performed in such a way to isolate the phenomenon of interest as much as possible. Heat-transfer coefficients (not available otherwise due to the use of unique NASA foam insulation for superior adiabatic conditions), for

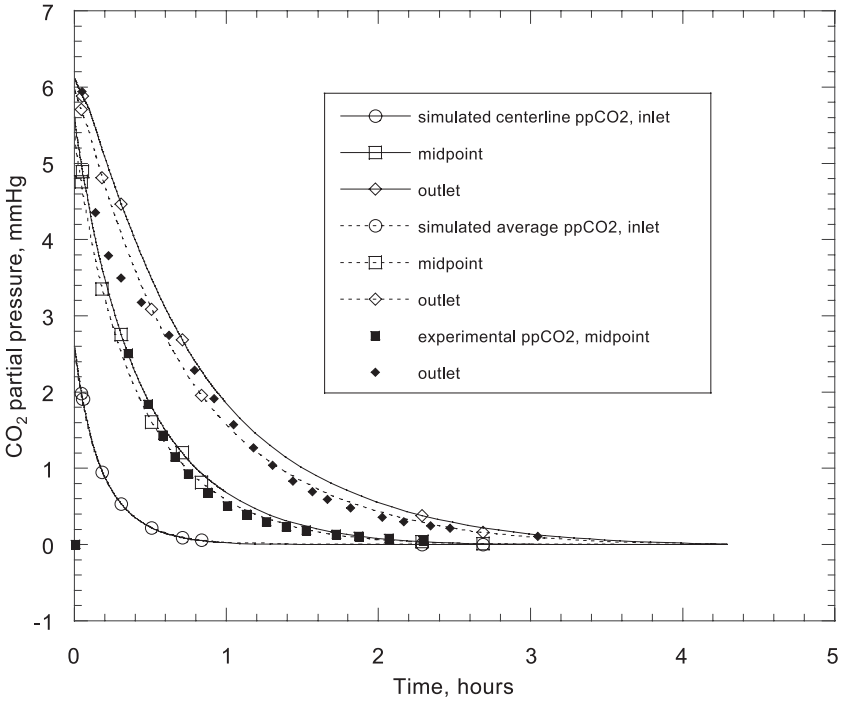

Figure 4. CO_2 desorption comparisons test with two-dimensional results.

Marcel Dekker, Inc.
270 Madison Avenue, New York, New York 10016

example, were obtained by flowing dry, heated nitrogen through a sorbent bed desorbed in the presence of nitrogen. Nitrogen gas was used since it is the main carrier gas. The adsorption affinity of nitrogen on 5A zeolite is negligible at high temperature, therefore, the heat generated during the dry-heated nitrogen through the column is minimal. Also, the curve fitting of experimental and model results was done at the later portion of curve where the temperature is high. However, the obtained heat-transfer coefficients fit the entire curve fairly accurately.[2]

The second use of the MSMBT is to verify, following ascertaining the of empirical values, the accuracy of the model under conditions similar to those expected in *the International Space Station Alpha (ISSA)*. This consists of comparing a series of MSMBT runs at varying conditions to the results of the computer model run at the same conditions. Of special interest is the capability of the model to predict transient bed

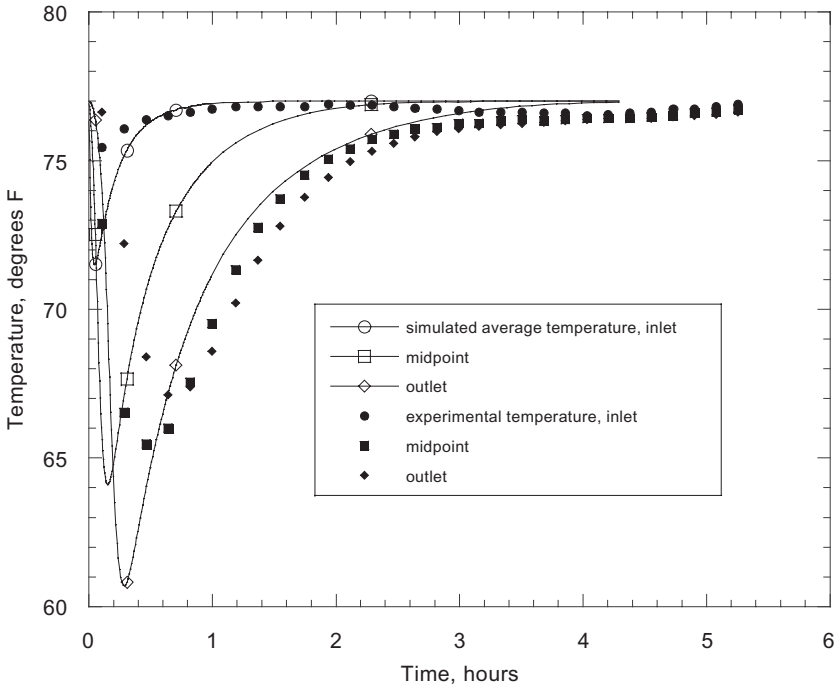

Figure 5. CO_2 gas temperature desorption comparison test with two-dimensional results.

MARCEL DEKKER, INC.
270 Madison Avenue, New York, New York 10016

temperature and partial pressure for conditions not used to obtain the empirical values.

COMPUTER MODEL VERIFICATION

Carbon Dioxide Single Component Adsorption

The test results of were used to verify the two-dimensional bed models for carbon dioxide adsorption. Test specifications are shown in Table 1. Two phenomenon were observed to occur during this adsorption test, which are not generally accounted for in mathematical models of this type. The first phenomenon is the significance of bed channeling in the 1.875-inch ID cylindrical column with sorbent pellets of 8 to 12 mesh (approx. 2mm in diameter). The existence of significant bed

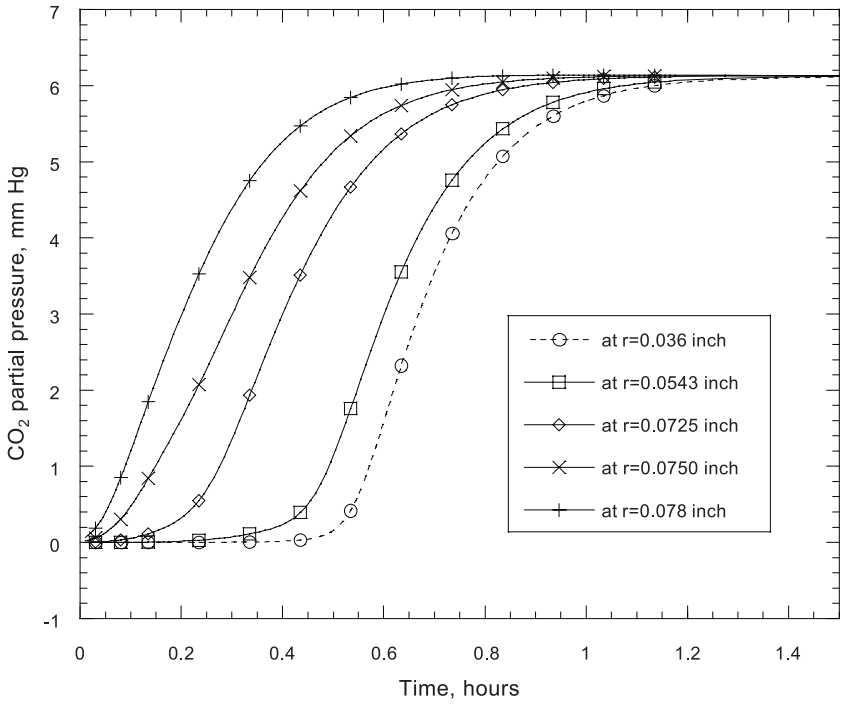

Figure 6. Calculated CO_2 breakthrough at the outlet of the bed for different radial points.

channeling is evident in Figure 1, which shows the breakthrough of CO_2 in the column. Note the discrepancy in the breakthrough at the material exit centerline (labeled ''Outlet'') from a point 5-inches downstream of the material exit (''Outlet Beads''). The downstream point measures all gas exiting the column mixed via turbulence through 5 inches of 3-mm glass beads. Consistent with the assumption of flow channeling at the column wall, the breakthrough is earlier for the mixed gas than that at the centerline of the column. The two-dimensional model was developed to account for the channeling, and to aid in derivation of a technique to intelligently apply a channeling factor to the more CPU efficient single dimension models.

The second phenomenon observed is the importance of including nitrogen co-adsorption for accurate modeling of the carbon dioxide breakthrough with nitrogen as the carrier gas, as it was discussed in previously.[1]

Model inputs are shown in Table 1. Pellet specific heat, is based on Davison Chemical Co. supply.

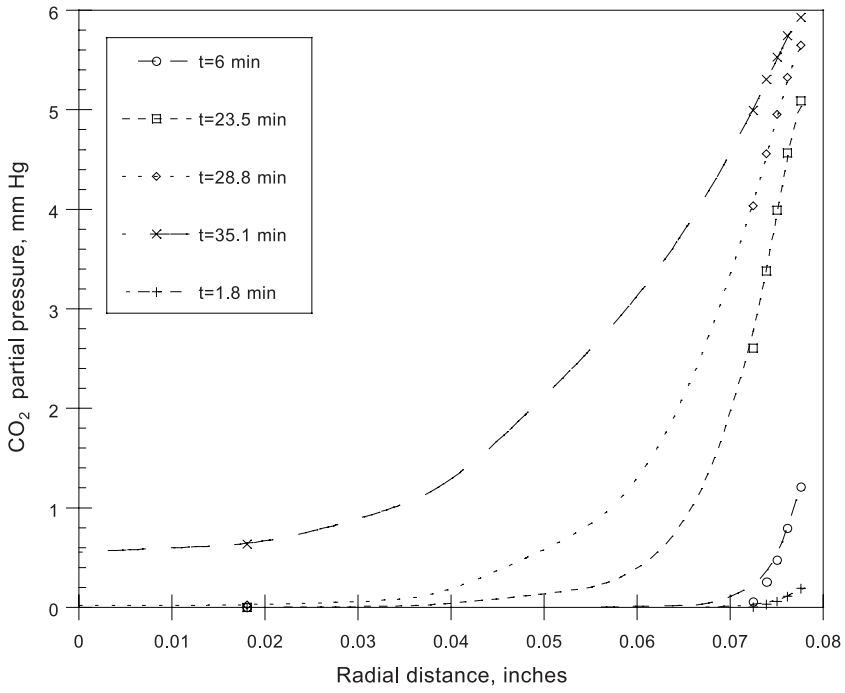

Figure 7. Calculated CO_2 adsorption concentration at the outlet of the bed for different times along the radial direction.

MARCEL DEKKER, INC.
270 Madison Avenue, New York, New York 10016

Two-Dimensional Model Verification

The determination of input values, mass-transfer coefficients, and verification of the two-dimensional single-and multicomponents material flow-through adsorption and desorption model is described in this section.

Carbon Dioxide Adsorption

Results of the model comparison of CO_2 single component are shown in Figures 2 and 3. As is evident, the comparison is very favorable. Note that two sets of model data are presented; averaged data and centerline data. The centerline data is the central node radially and the last bed material node axially. The simulated two-dimensional centerline data matches the one-dimensional simulated results.[1] Averaged data is also at the last bed node axially, but is an average of all the radial nodes. The averaged data is thus representative of gas after mixing in the glass beads,

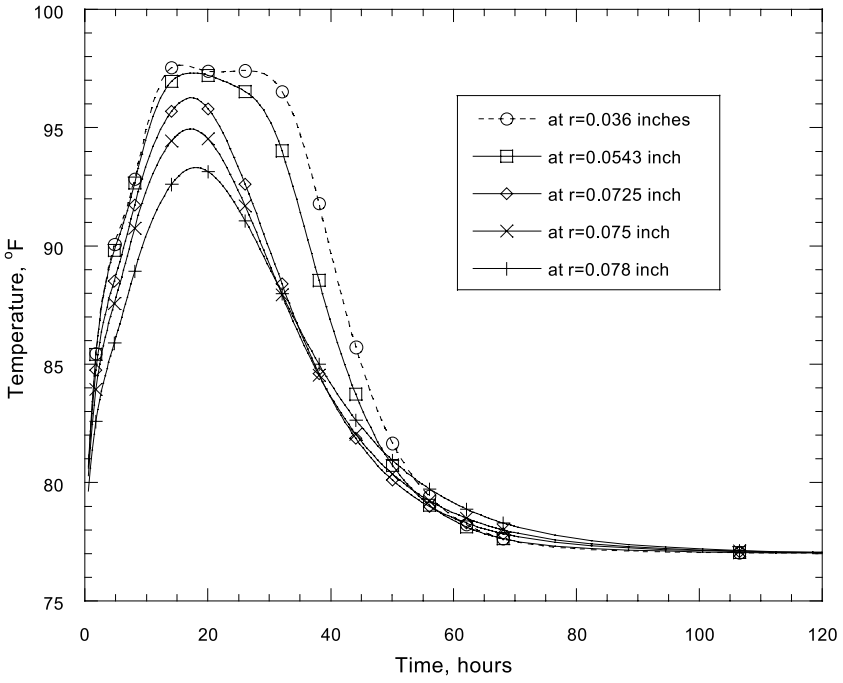

Figure 8. Calculated adsorption temperature at the outlet of the bed at different radial locations.

Marcel Dekker, Inc.
270 Madison Avenue, New York, New York 10016

or the test data labeled ''Outlet Beads.'' The centerline data is representative of test data taken at the center of the bed radially and at the end of the bed material axially.

Based on the above discussion, it is expected that centerline data—the line with filled markers in Figure 1—will compare with the small circular markers. As seen from the figure, this comparison is indeed favorable. Average data should be compared with the small triangular markers, and once again, this is a favorable comparison. As a result, it can be inferred that the two-dimensional model does correctly model the channeling observed in this test.

As seen from Figure 3, the temperature comparison is also favorable. The increase in fidelity of the two-dimensional model is evident by comparison of Figure 4, with the results from the one-dimensional model.[1] The two-dimensional simulation more closely follows the actual temperature peak, both in time and in magnitude.

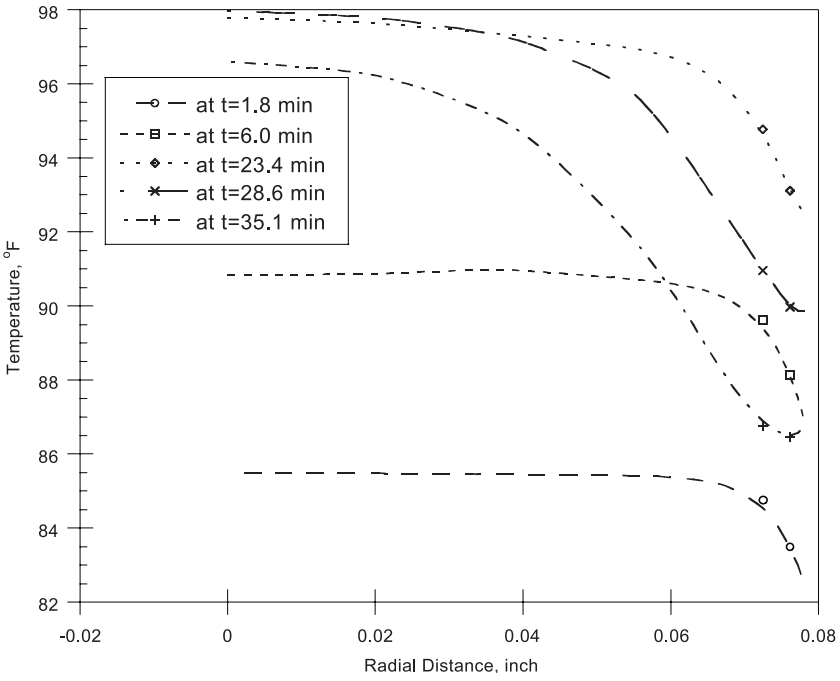

Figure 9. Calculated adsorption temperature at the outlet of the bed for different times along the radial direction.

MARCEL DEKKER, INC.
270 Madison Avenue, New York, New York 10016

The short time of breakthrough allows it to use ideal adsorption solution theory (IAST), even though it takes more CPU time than using the Langmuir isotherm. A mass transfer coefficient of 0.017 ft/hr was used in predicting the CO_2 breakthrough curve.

Carbon Dioxide Desorption

Results of the model comparison are shown by the solid lines in Figures 5 and 6. The model prediction of centerline and average breakthrough definitely matches the obtained experimental data. The temperature profile result of the two-dimensional model also estimates the experimental data fairly well. The few degree discrepancy between the model and experimental data is largely due to predicting the heat-transfer coefficients between the packed bed and the wall and between the wall and the surrounding. The two parameters have a strong effect on radial

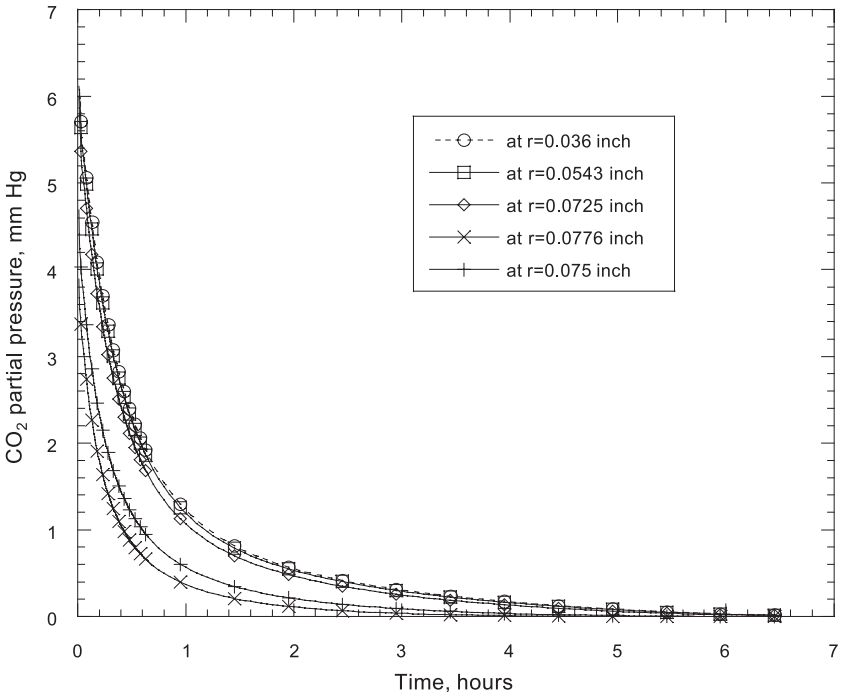

Figure 10. Calculated CO_2 desorption concentration at the outlet of the bed for different radial points.

Marcel Dekker, Inc.
270 Madison Avenue, New York, New York 10016

temperature profile. Trial and error must be performed to obtained the corrected values. The IAST was used to predict the CO_2/N_2 mixture isotherm. A mass-transfer coefficient of 0.017 ft/hr was used for the prediction of breakthrough curve.

CO_2 Temperature and Concentration of Model Results in Radial Direction

The influence of porosity variation and the no-slip flow on temperature and concentration fronts of CO_2 adsorption along the radial direction is significant, as is shown in Figures 6 and 7. The early breakthrough of CO_2 increases from the central line up to the wall of the packed-bed column. It is evident that the dispersion in axial direction is lesser toward the wall than the center of the column, specially at beginning of the breakthrough. Figures 8 and 9 show the model results of temperature variation at outlet of adsorbents in the radial direction. Even though the effort made to make the

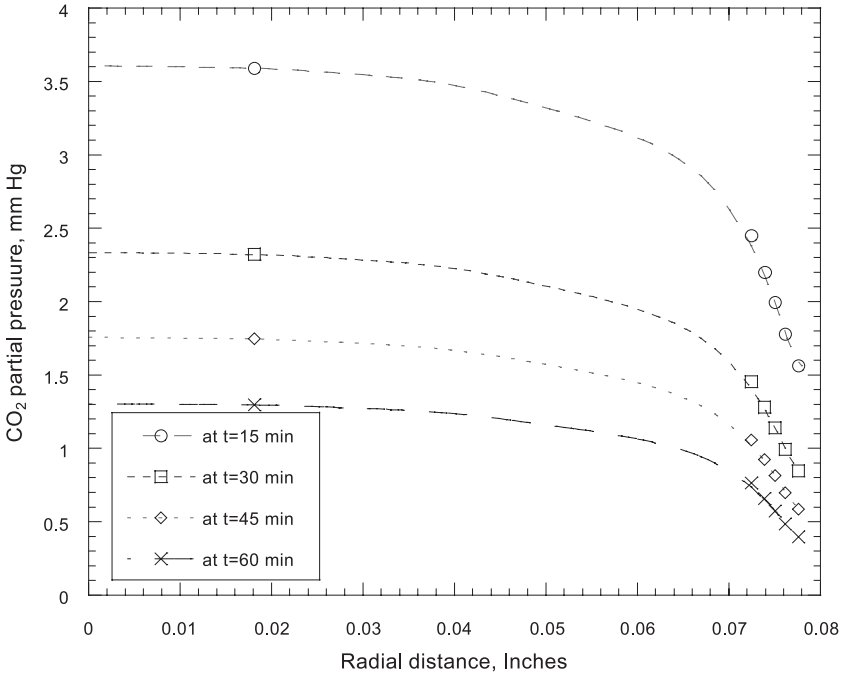

Figure 11. Calculated CO_2 desorption concentration at the outlet of the bed for different times along the radial direction.

MARCEL DEKKER, INC.
270 Madison Avenue, New York, New York 10016

column adiabatic the temperature variation in the radial direction is significant. Although, the larger porosity near the wall causes an early breakthrough of the CO_2, but the lower temperature at the wall makes the CO_2 to be adsorbed more because of a higher affinity of adsorption at lower temperature. It should be noted that the porosity variation is a decaying exponential phenomenon and, therefore, more pronounce within 10 percent of the wall radius. However it occupies where the surface fraction is the largest.

Figures 10 and 11 present the concentration breakthrough for CO_2 desorption for different points along the radial direction. The effect of porosity variation and the no-slip flow on stripping the CO_2 is that it takes longer to strip the center of the column from CO_2 than close to the wall. Figures 12 and 13 show the model results of concentration and temperature variations at outlet of the sorbent with respect to radial position. It is also evident that because the centerline is more condensed, the temperature is lower because of the effect of heat of desorption.

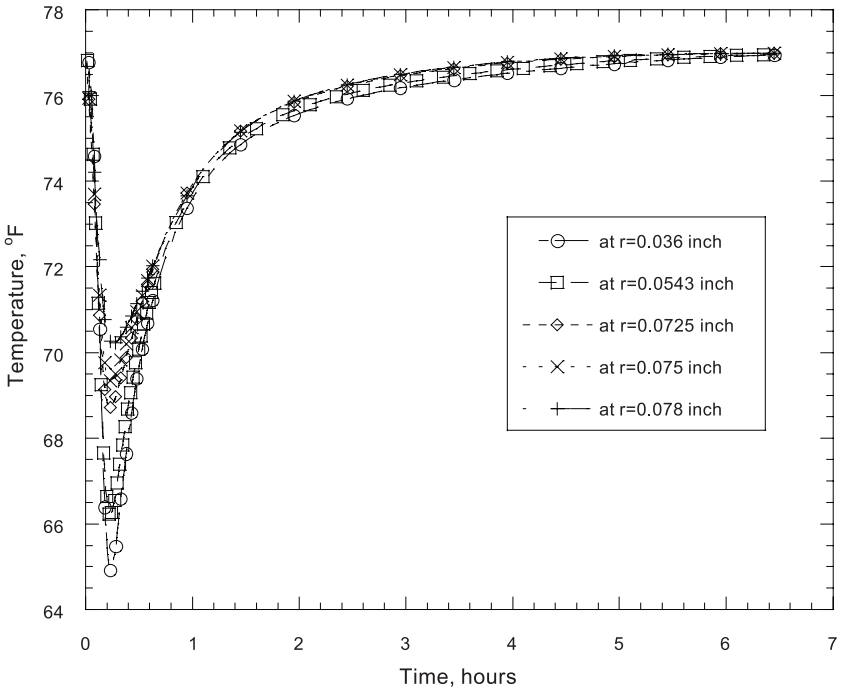

Figure 12. Calculated desorption temperature at the outlet of the bed at different radial locations.

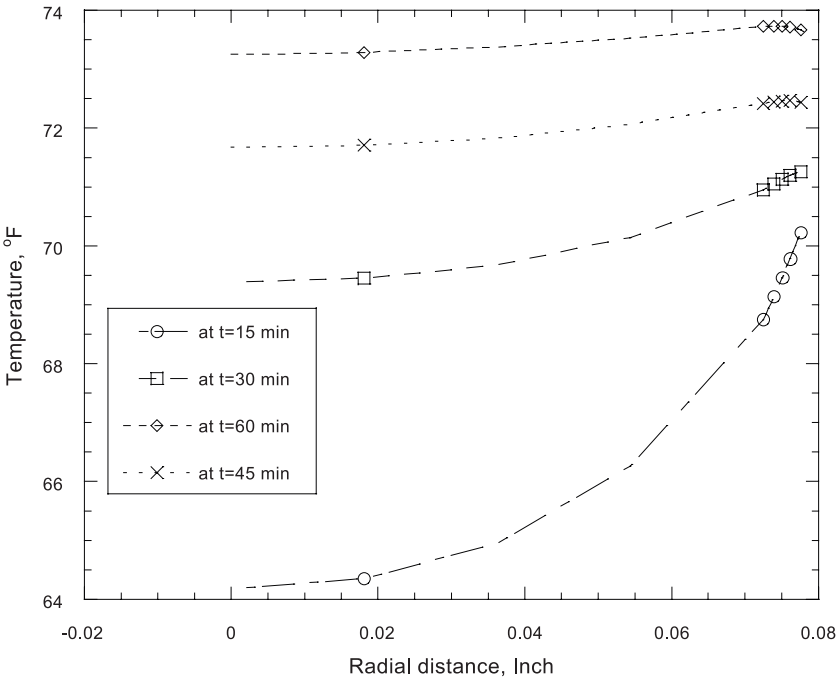

Figure 13. Calculated adsorption temperature at the outlet of the bed for different times along the radial direction.

CONCLUSIONS

Based on analytical and experimental investigation of two-dimensional connective flows in porous media, the following conclusions are drawn.

- The experimental results from the laboratory scale-fixed bed adsorber are quantitatively consistent with the one-dimensional model at the column center. The average concentrations of cross-sectional bed obtained by test result deviates from the column center concentration in a one-dimensional model appreciably and are fairly good with a two-dimensional model. This indicates that the strong effects of porosity variation along the radial direction of column bed on the temperature, concentration, and velocity field can be modeled by non-slip flow model.
- A linear driving force mass-transfer model for the solid phase provides a reasonable fit to experimental adsorption data.

- The average and centerline CO_2 concentration breakthrough and temperature profiles of the test results matches the two-dimensional model reasonably well.
- It is evident that in modeling the packed bed column with one-dimensional flow, an average velocity and porosity should be considered so that at least some of the effects of radial variation of these two parameters are introduced into the one-dimensional model.

NOMENCLATURE

a	Surface area of pellets per unit volume of pellet ft^2/ft^3
C	Gas phase concentration of i^{th} component in the bulk, lb mole/ft^3
C	Constant in Darcy equation
$C_{i,0}$	Gas phase concentration of i^{th} component at boundary or initial condition, lb mole/ft^3
C_{pg}	Heat capacity of gas phase, Btu/lbm-R
C_{ps}	Heat capacity of solid particle, Btu/lbm-R
C_{pw}	Heat capacity of column wall, Btu/lbm-R
d, d_t	Column diameter, ft
d_p	Particle diameter, ft
D	Diffusivity, ft^2/hr
D_o	Stagnant diffusivity, ft^2/hr
D_l	Axial diffusion, ft^2/hr
$D_{i,j}$	Binary molecular diffusion, ft^2/hr
D_{mi}	Molecular diffusion in mixture, ft^2/hr
D_f	Fluid flow diffusivity, ft^2/sec
$D_{eff,x}$	Effective axial diffusivity, ft^2/sec
$D_{eff,r}$	Effective radial diffusivity, ft^2/sec
$D_{f,x}$	Axial diffusivity of fluid flow, ft^2/sec
$D_{f,r}$	Radial diffusivity of fluid flow, ft^2/sec
d_w	Bed diameter, ft
G	Superficial mass velocity, lb_m/ft^2 hr
h_o	Effective heat-transfer coefficient for column insulation, Btu/ft^2-hr
h_w	Heat-transfer coefficient between the gas and the column wall, Btu/ft^2-hr
h_s	Heat-transfer coefficient between the gas stream and the sorbent, Btu/ft^2-hr
K	Constant in Darcy equation
k_f	Fluid flow axial conductivity, dispersion, Btu/ft-hr-R
k_o	Stagnant thermal conductivity, Btu/ft-hr-R
$k_{eff,x}$	Effective axial conductivity, Btu/ft-hr-R

Marcel Dekker, Inc.
270 Madison Avenue, New York, New York 10016

k_{es}	Effective overall mass-transfer coefficient, monodisperse particle, ft^2/hr
$k_{eff,r}$	Effective radial conductivity, Btu/ft-hr-R
$k_{f,x}$	Axial conductivity of fluid flow, Btu/ft-hr-R
$k_{f,r}$	Radial conductivity of fluid flow, Btu/ft-hr-R
$k_{s,x}$	Solid thermal conductivity in axial direction, Btu/ft-hr-R
$k_{s,x}$	Solid thermal conductivity in radial direction, Btu/ft-hr-R
k_{fi}	Fluid film mass-transfer coefficient of i^{th} component, ft/hr
$k_{eff,i}$	Effective mass-transfer coefficient of i^{th} component, ft/hr
L	Column length, ft
M_i	Molecular weight of adsorbate i, lb/lb mole
n	Number of component
N_{Pe}	Peclet number, $c_{pg}\rho_g u/k$
N_{Re}	Reynolds number, $d_p\rho_g u/\mu$
N_{sc}	Schmidt number, $\mu/D\rho_g$
P	Total pressure, mm Hg or lbf/ft^2
P_i	Partial pressure of component i, mm Hg or lbf/ft^2
q	Amount adsorbed in the solid, lb moles/ft^3 of solid
q^*_i	Solid phase concentration of i^{th} component in equilibrium with gas phase, lb moles/ft^3 of solid
$\bar{q}_i$	Volume average solid phase concentration of component i, lb moles/ft^3 of solid
r	Radial position, ft
R	Ideal gas constant 555 mm Hg ft^3/lb mol R
R_i	Inside wall diameter of column, ft
R_o	Outside wall diameter of column, ft
t	Time, hr
T	Temperature R
T_o	Ambient temperature, R
T_g	Gas temperature, R
T_w	Wall temperature, R
T_s	Solid temperature, R
u	Interstitial velocity, ft/hr
x	Axial position
x_i	Mole fraction of i^{th} component in the solid phase
y_i	Mole fraction of i^{th} component in the gas phase

Greek

$\alpha\beta$	Constant in effective conductivity equation
ε	External bed void volume
λ	Constant in effective conductivity equation

MARCEL DEKKER, INC.
270 Madison Avenue, New York, New York 10016

ϕ	Constant in stagnant conductivity equation
ρ_{pg}	Density of gas phase, lb mole/ft^3
ρ_s	Density of solid phase, lb/ft^3
ρ_w	Density of column wall, lb mole/ft^3
μ	Fluid viscosity
σ	Emissivity
ΔH	Heat of adsorption, BTU/lb of solid

Subscripts

e	Effective
eff	Effective
f	In the fluid phase
i	ith component
o	Outside, initial
pg	Gas phase
s	Surface
t	Total
w	Wall

Superscripts

-	Average value
*	Equilibrium value

REFERENCES

1. Mohamadinejad; Knox. Experimental and numerical investigation of adsorption/desorption in packed sorption beds under ideal and non-ideal flows. Sep. Sci. Technol. **2000**, *35* (1), 1–22.
2. Mohamadinejad, H. The adsorption of $Co_2/H_2o/N_2$ on 5a zeolite and silica gel in a packed column in one and two-dimensional flows. Ph.D Thesis; University of Alabama in Huntsville, 1999.
3. Benenati, R.F.; Brosilow, C.B. Void fraction distribuation in beds of spheres. AICHE J. **1962**, *8*, 359–361.
4. Chu, C.F. Flow in pcked tubes with a small tube to particle diameter ratio. AICHE J. **1989**, *35* (1), 148–158.
5. Vortmeyer, D.; Michael, K. The efffect of nonuniform flow distribution on concentration profiles and breakthrough curves of fixed bed adsorber. Chem. Eng. Sci. **1985**, *40*, 2135–2138.
6. Cohen, Y.; Metzner, A.B. Wall effect in laminar flow of fluids through packed beds. AICHE J. **1981**, *27* (5), 705–715.

Marcel Dekker, Inc.
270 Madison Avenue, New York, New York 10016

7. McGreavy, C.; Foumeny, E.A. Characterization of transport properties for fixed beds in terms of local bed structure and flow distribution. Chem. Eng. Sci. **1986**, *41*, 787–797.
8. Roblee, L.H.S.; Baird, R.M.; Tierney, J.W. Radial porosity variation in packed beds. AICHE J. **1958**, *4*, 460–464.
9. Nield, D.A.; Bejan, A. *Convection in Porous Media*; Springer-Verlag: New York, 1992.
10. Newman, J. Numerical solution of coupled, ordinary differential equations. Ind. Eng. Chem. Fundam. **1968**, *7*, 514–517.
11. Bird, R.B.; Stewart, W.E.; Lightfoot, E.N. *Transport Phenomena*; Jon Wiley & Sons, Inc: New York, 1960.
12. Slattery, J.C.; Bird, R.B. AICHE J. **1958**, *4*, 137–142.
13. Ruthren; Sargent, D.R.; Whitford, C.J. Diffusion of carbon dioxide in type 5A molecular sieve. In *Molecular Sieve II (Advances in Chemistry Series 102)*; American Chemistry Society: Washington, DC, 1971.
14. Do, D.D. Sorption of bimodal microporous solid with an irreversible isotherm. Chem. Eng. Sci. **1989**, *44* (8), 1707–1713.
15. Greg, D.R.; Ruthven, D.M. The effect of concentration dependent of diffusivity on zeolite sorption curve. Trans. Faraday Soc. **1972**, *27*, 413–423.
16. Sargent, D.R.; Whitford, C.J. Diffusion of carbon dioxide in type 5A molecular sieve. In *Molecular Sieve II (Advances in Chemistry Series 102)*; American Chemistry Society. Washington, DC, 1971.
17. Vafai, K.; Tien, C.L. Boundry and inertia effect on convective mass transfer in porous media. Int. J. Heat Mass Transfer **1982**, *24*, 195–203.
18. Ergun, S. Fluid flow through through packed column. Chem. Eng. Prog. **1952**, *48*, 89–94.
19. Kunii, D.; Smith, J.M. Heat transfer characteristics of porous rocks. AICHE J. **1960**, *6*, 97.
20. Fahien, R.W. Ph.D thesis; Purdo University, 1954.
21. Baron, T. Chem. Eng. Progr. **1952**, *48*, 118.
22. Yagi, S.; Kunii, D., 1957.
23. Yagi, S.; Kunii, D.; Wakao, N. AICHE J. **1960**, *6*, 543.
24. Hunt, M.L. Non-darcian convection in packed-sphere and fibrous media. PhD thesis; Univ of Calif, Berkeley, 1987.
25. Argo, W.B.; Smith, J.M. Chem. Eng. Prog. **1953**, *49*, 443.
26. Fahien; Smith.
27. Kunii, D.; Suzuki, M.; Ono, N. Heat transfer from wall surface to packed beds at high reynolds number. J. Chem. Eng. Jpn. **1968**, *1*, 21–26.
28. Suzuki, M. *Adsorption Enigineering*, 1st Ed.; Elsevier Science Publishing Company: New York, 1990.

MARCEL DEKKER, INC.
270 Madison Avenue, New York, New York 10016

29. Newman, J. *Numerical Solution Of Coupled, Ordinary Differential Equations (UCRL-17739)*; Lawrence Radiation Laboratory: University of California, Berkeley, August 1967.
30. Sewell, G. *The Numerical Solution of Ordinary and Partial Differential Equations*; Acadamic Press: San Diego, CA, 1988.
31. Darcy, H. *Les Fontains Publiques de la ville de Dijon*; Damont: Paris, 1956.
32. Glueckauf, E. Theory of chromotography-part 10. Trans. Faraday Soc. **1955**, *51*, 1540.
33. Smith, J.M. *Chemical Engineering Kinetics*, 3rd Ed.; McGrow-Hill Book Compony: New York, 1981.

Received May 1999
Revised September 1999